



Corrosion behaviour of the Al-2.1-Mg-1.8-Si alloy in chloride solution

YAYA ZHENG, BINGHUI LUO*, CHUAN HE, ZHIWEI REN, SHUAI WANG and YUAN YIN

College of Materials Science and Engineering, Central South University, Changsha 410083, People's Republic of China

*Author for correspondence (luobinghui@csu.edu.cn)

MS received 16 January 2019; accepted 1 May 2019; published online 10 July 2019

Abstract. The corrosion behaviours of Al-Mg-Si alloys were studied in different Cl^- concentrations by means of scanning electron microscopy, transmission electron microscopy and electrochemical experiments. The results show that the corrosion behaviours of Al-Mg-Si alloys are closely related to the Cl^- concentration. With an increase in Cl^- concentration, the corrosion rate increases sharply by facilitating the process of chemical and electrochemical reactions. In 2.0 wt.% NaCl solution, slight pitting corrosion occurred around the MgSi phase, but corrosion trenching was not found around the Fe-Mn-Si phase. In 3.5 wt.% NaCl solution, the alloy appeared localized corrosion dominated by intergranular corrosion attack. In 5.0 wt.% NaCl solution, the alloy presented serious overall corrosion, and the passivation platform of the polarization was not obvious. Furthermore, an appropriate corrosion mechanism according to polarization and electrochemical impedance spectroscopy was proposed for the Al-Mg-Si alloy in NaCl solution. In addition, the corrosion rate influenced by different Cl^- concentrations was discussed in detail.

Keywords. Al-Mg-Si alloy; corrosion behaviour; Cl^- ; passivation film.

1. Introduction

Corrosion, a great challenge faced by almost all industries can be considered as one of the worst technological calamities [1,2]. Aluminium alloys are generally resistant to corrosion in aqueous solutions because of their presence of passivation film [3–5]. Some literature studies pointed out that the passivation film of aluminium alloys is a kind of poor semiconductor [6,7]. The cathodic reaction occurs on some micron-sized dispersoids or impurity particles [8]. The anodic reaction occurs on some second phases with low potential or aluminium matrix. The chemical composition, the second phase type and the surface condition of the alloy have a significant influence on the corrosion resistance of the passivation film [9]. Extensive studies researched on the effects of element on corrosion behaviour of Al-Mg-Si alloys. The existence of some intermetallic compounds (Al_2Cu , FeAl_3) and single elements (Cu, Si) can easily result in the formation of local electrochemical batteries within the aluminium matrix [10]. Zheng *et al* [11] studied the corrosion process of Al-Mg-Si alloys in NaCl solution, indicating that the corrosion attack starts from the area around the second phase. Nabhan [12] studied the effects of the pH value and the heat treatment on the corrosion behaviours of aluminium alloys. The results indicated that alloying elements have an influence on the corrosion resistance of the passivation film.

The corrosion process of aluminium alloys in aqueous solutions is very complicated. Except for alloying elements and microstructures, corrosion medium is another important

factor with regard to the corrosion performance of aluminium alloys by influencing the stability of the passivation film [13–15]. To find a suitable method for enhancing the corrosion resistance of Al-Mg-Si alloys, extensive studies associated with corrosion susceptibility in different corrosion solutions have been conducted. Tan *et al* [16] studied the corrosion electrochemical characteristics of the Al-Mg alloys in seawater, and the results illustrated that the anodic polarization and the increasing NaCl concentration were beneficial to the formation of active points, which results in pitting corrosion. Guan *et al* [17] investigated the intergranular corrosion behaviour of Al-Mg-Si alloys with different Mg/Si in 0.6 M NaCl solution (pH 3.5) via electrochemistry tests. The results indicated that corrosion was initiated around MgSi precipitates. Huang *et al* [18] and Shi *et al* [19] found that the corrosion behaviours were significantly different between alkaline solutions and neutral/acidic solutions. Corrosion behaviour of Al-Mg-Si alloys is strongly affected by these different corrosion conditions, and thus, it is difficult to make a comparative analysis. To date, there is no detailed study concerning the effects of Cl^- concentration on the corrosion behaviour of Al-Mg-Si alloys and no definite theory for analysing the corrosion behaviour has been yet established.

Consequently, this work presents a study related to the effects of Cl^- concentration on corrosion behaviours of Al-Mg-Si alloys by evaluating the corrosion morphology and corrosion products. The polarization curve and electrochemical impedance spectroscopy (EIS) were employed that aimed at deducing the corrosion mechanism. An appropriate

corrosion mechanism of the Al–Mg–Si alloy in different NaCl solutions is proposed, and a possible corrosion process occurring in the passivation film is discussed. In addition, this study particularly focusses on the corrosion rate influenced by different Cl^- concentrations.

2. Experimental

2.1 Sample preparation

The experimental alloys were produced in an arc melting furnace. High-purity Al and Mg, Al–Si and other master alloys were used as raw materials. The compositions of the obtained alloys for analyses are 2.1 wt.% Mg, 1.8 wt.% Si, 0.3 wt.% Cr, 0.3 wt.% Mn, 0.3 wt.% Zr, 0.2 wt.% Ti, 0.1 wt.% Fe and the rest are Al and inevitable impurities. The heat-treatment process of the alloy was homogenized at 530°C for 12 h; solid solution was treated at 540°C for 2 h; quenched in ambient water and then, underwent artificial ageing treatment at 180°C for 5 h.

2.2 Corrosion test

Before each corrosion test, the exposed surface of the sample was polished and washed with ethanol and distilled water, respectively, and then, dried in air. To avoid prolonged exposure time in the atmosphere, samples were tested immediately after drying. The corrosion solutions are prepared by distilled water and sodium chloride (analytical grade reagent). Various NaCl solutions with concentrations of 2, 3.5 and 5 wt.% were prepared, respectively.

Open-circuit potential (OCP), potentiodynamic polarization and EIS are performed using a three-electrode system. The reference electrode was the saturated calomel electrode. The auxiliary electrode was the platinum plate electrode, and the working electrode was the tested sample. The exposed area of the sample was 1×1 cm. The scanning interval was $-1.6 \sim 0.2$ V, and the scanning rate was 2 mV s^{-1} . After the potentiodynamic polarization test, the electrochemical kinetic parameters were calculated by Nova.2.1 software. EIS was obtained at the OCP by applying a sinusoidal voltage signal of 10 mV in a frequency range of 10^{-2} – 10^5 Hz. EIS data were analysed by ZSimp Win software.

2.3 Microstructure characterization

The microstructure and corrosion morphology of the tested alloys were observed by scanning electron microscopy (SEM) in a Sirion-200 microscope. The grain boundary precipitates were observed by transmission electron microscopy (TEM) on a Tecnai G2 20 instrument at an operating voltage of 200 kV.

3. Results and discussion

3.1 Microstructure

The type and distribution of the second phase play key roles in the corrosion properties of the alloy. Figure 1 shows the grain boundary microstructure and corresponding energy dispersive spectroscopy (EDS) results. There are two contrast typical constituent particles with the size ranging from 5 to 20 μm in SEM with back-scattered mode. The EDS analyses exhibit that the main chemical elements of the white contrast phase (point 1) are Al, Si, Fe and Mn; the main chemical elements of the grey contrast phase (point 2) are Mg and Si with stoichiometry close to Mg_2Si . It has been verified that these micrometre-scale particles formed during the casting process. Some short rod-like precipitates exist in the grain boundaries with intermittent distribution, and the precipitate free zone is not obvious (figure 1c). According to its morphology and related literature [11], the rod-like precipitates can be determined as β' -phases. The β' -phase acts as an anode phase during corrosion, and preferentially be corroded before the Al matrix. However, because of their small size, many studies proved that the nano-precipitates have little effect on the corrosion process [20].

3.2 Electrochemical test

The OCP–time curves of the investigated alloys in NaCl solutions with different concentrations are shown in figure 2. In 2, 3.5 and 5 wt.% conditions, the initial potential value rapidly changes, following almost constant potential after a period of ~ 2300 , 1600 and 1000 s, respectively. The time to achieve a stable OCP value prolongs with an increase in the NaCl concentration. With an increase in the NaCl concentration, the OCP shifts to more negative values. The OCP value usually relates to the effectiveness of protecting passivation from corrosion. The time to reach a stable OCP value relates to the formation and activation of the oxide film in corrosion solution.

The potentiodynamic polarization curves of the alloys in different NaCl concentration solutions are presented in figure 3. The corrosion rate (V_{corr}) was calculated by the following formula:

$$V_{\text{corr}} (\text{mm y}^{-1}) = \frac{3270 \times M \times i_{\text{corr}}}{\rho \times Z},$$

where Q the density of the alloy (g cm^{-3}), m the atomic mass of the metal (Al) and Z the number of electrons transmitted by each atom. The calculation results are presented in table 1. The results indicate that with an increase in NaCl concentration, the E_{corr} shifts negatively, the polarization resistance (R_p) decreases sharply and the V_{corr} of the alloy increases. Therefore, the corrosion process is affected more by the anodic process rather than the cathodic process. It is

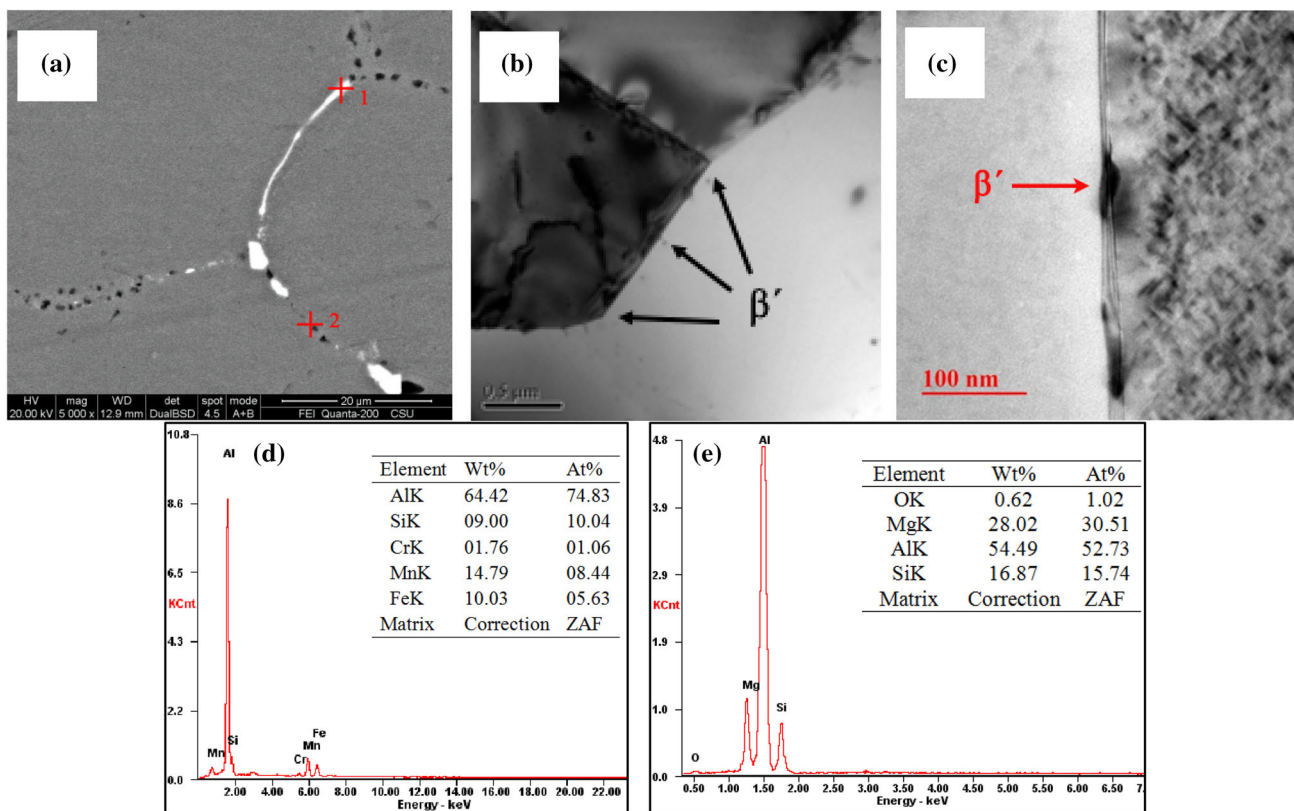


Figure 1. Grain boundary microstructure and corresponding EDS results. (a) Backscatter electron microscopy images; (b, c) TEM bright field images and (d, e) corresponding EDS results of the particles marked 1 and 2, respectively.

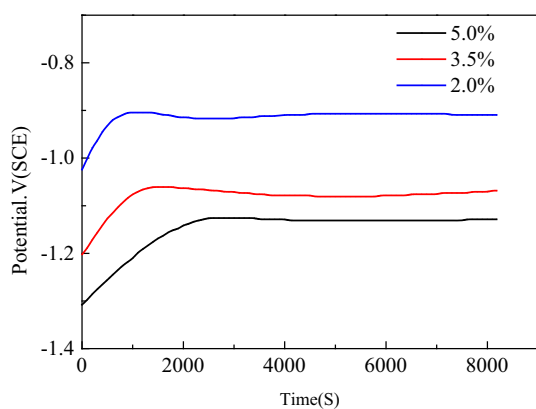


Figure 2. OCP-time for the Al-Mg-Si alloys in different NaCl concentration solutions.

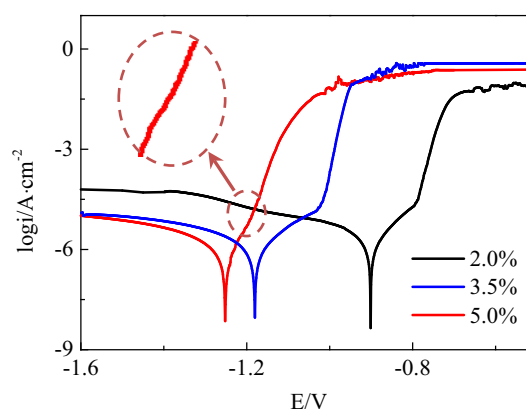


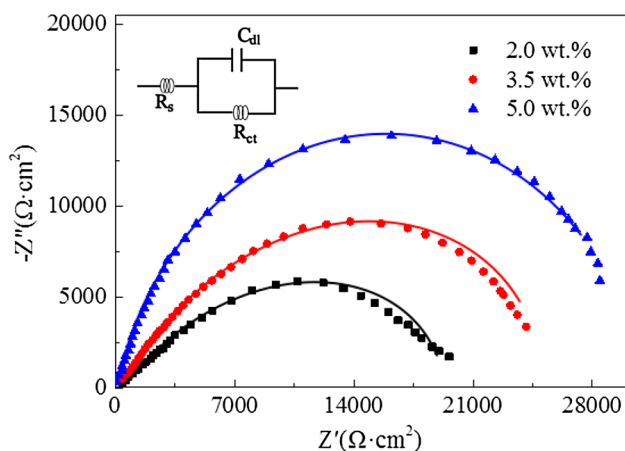
Figure 3. Polarization curves of the Al-Mg-Si alloys in NaCl solution at various concentrations of NaCl.

worthy of note that with an increase in the Cl⁻ concentration, the slope of the passivation platform increases. When the NaCl concentration reaches 5.0 wt.%, $E_{corr} = E_{pit}$. The passivation characteristics were not obvious, which indicates that the main corrosion form is pitting corrosion. In addition, β_a and β_c almost remain unchanged, indicating that the corrosion mechanism of the alloys did not change.

To further clarify the corrosion mechanism of the alloys in NaCl solution, the Nyquist plots with regard to various concentrations of NaCl solution and the equivalent circuit are shown in figure 4. The general shape of these curves is very similar and the EIS diagram shows single capacitive semi-circles. Thus, the corrosion mechanism did not change. The corrosion process is mainly controlled by charge transfer and

Table 1. Related parameters of the polarization curve and EIS tests of the Al–Mg–Si alloys.

NaCl concentration (wt.%)	E_{corr} (mV)	E_{pit} (mV)	i_{corr} (mA cm^{-2})	β_a (mV dec^{-1})	β_c (mV dec^{-1})	R_p ($\Omega \cdot \text{cm}^2$)	V_{corr} ($\mu\text{m year}^{-1}$)	R_{ct} ($\Omega \cdot \text{cm}^2$)	C_{dl} ($\Omega^{-1} \text{cm}^{-2} \text{s}^{-1}$)
2	-0.91	-782 ± 3	720 ± 4	85	124	28,050	7.84	26,874	1.25×10^{-4}
3.5	-1.18	-108 ± 3	1050 ± 5	71	131	22,103	11.43	21,316	1.03×10^{-4}
5	-1.25	-1250 ± 3	1110 ± 8	79	126	14,528	12.09	13,895	0.97×10^{-4}

**Figure 4.** Nyquist plots for the Al–Mg–Si alloy in various NaCl concentration solutions. The experimental data are shown as points and the fitting results as lines.

could be attributed to the oxide layer formed above the Al–Mg–Si alloys. R_s represents the ohmic solution resistance of the electrolyte. R_{ct} and C_{dl} are the charge transfer resistance and electrical double layer capacitance of the original surface at a high frequency, respectively, which correspond to the electrochemical process at the alloy/solution interface. It is noteworthy that the R_{ct} value decreases with a decrease in R_p . The C_{dl} increases with an increase in the NaCl concentration, indicating decreasing efficiency of protective ability of the oxide film.

3.3 Corrosion morphology

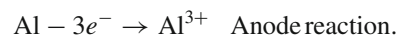
The corrosion morphology of the investigated alloys after immersion in NaCl solutions with different concentrations is shown in figure 5. The corrosion morphology of the investigated alloys immersed in 2 wt.% NaCl solution for 12 h is shown in figure 5a and d. The alloy exhibits slight pitting corrosion around MgSi particles, which is confirmed by the EDS results that the elements of the residue MgSi particles are O, Si, Al and Mg (figure 5g). However, no other corrosion sign appears around the Fe–Mn–Si particles. The alloy suffered serious pitting corrosion and even developed into a typical intergranular corrosion (figure 5b and e). The detailed evolution process is expounded by Zheng *et al* [11]. EDS

analysis of point 2 (figure 5h) shows that besides Al, Si and Mg, the residue particles also contain high content of Mn and Fe, which indicates the corrosion of Mn–Fe intermetallic in 3.5 wt.% NaCl solution. But the corrosion morphology of the alloy presents an obvious difference in 5 wt.% NaCl solution as shown in figure 5c and f. Not only serious intergranular corrosion occurs within the alloy, but also much micro-pits corrosion can be detected on the alloy matrix surface. These micro-pits may result from dissolution of some of the MgSi dispersoids. EDS analyses indicate that the corroded matrix is rich in elements of O, Al and Mg, and O content is high (figure 5i). This could be due to the corrosion of the oxide film. An increase in NaCl concentration leads to faster dissolution of the oxide film than its formation.

The electrochemical results and corrosion morphology analysis show that the corrosion process is controlled by the oxide layer. As such, analysis of the above results provides an opportunity to further expound the correlation between the Cl^- concentration and the corrosion rate of Al–Mg–Si alloys. For multicomponent Al alloys, because of the uneven chemical and physical properties of the oxide film, corrosion originates from the weak protection point, for example, around MgSi phases, Fe–Mn–Si particles and β' precipitates. In neutral aqueous solution, Cl^- can be adsorbed onto the interface between the passivation film and the water solution, and then penetrates through the passivation film into the weak protection point. The electric field, which destroys protective ability of the oxide film, results in the chemical and electrochemical dissolution of the oxide film and the alloy matrix. The chemical dissolution mechanism of the alloy is as follows [21,22]:



The faster electrochemical corrosion also exists. The cathodic and anodic reaction equations are respectively shown below:



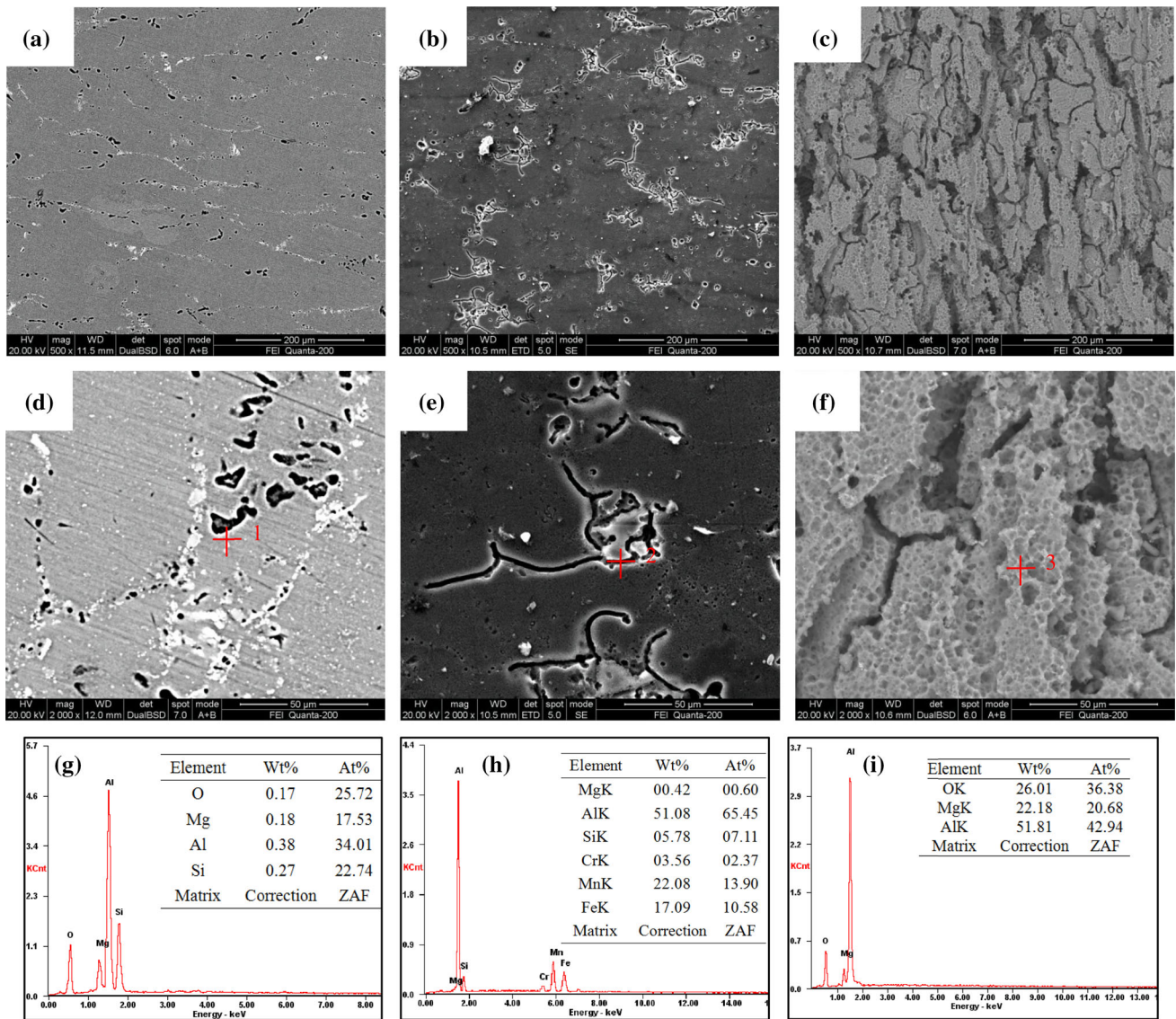


Figure 5. Corrosion morphology and corresponding EDS of the Al–Mg–Si alloy after immersion in NaCl solution with various NaCl concentrations for 12 h. (a, d) 2 wt.%; (b, e) 3.5 wt.%; (c, f) 5 wt.% and (g, h, i) corresponding EDS results of particles marked 1, 2 and 3, respectively.

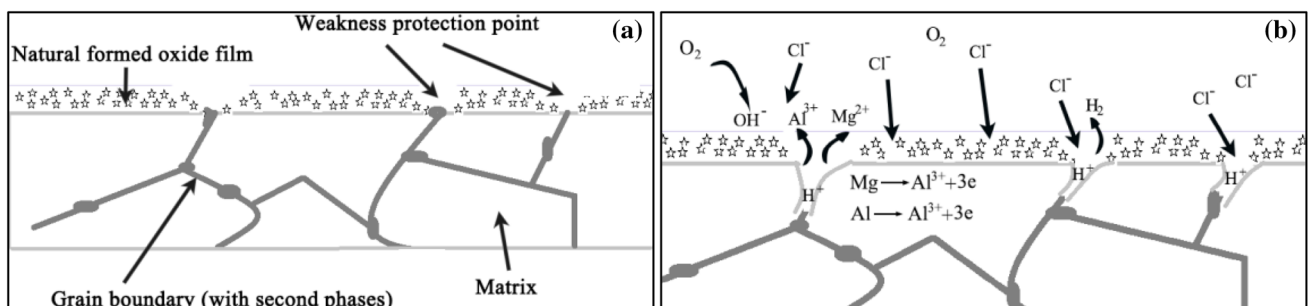
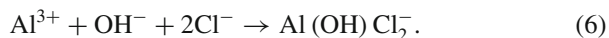
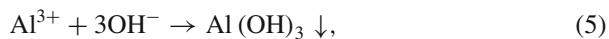


Figure 6. Schematic illustration of the corrosion of the Al–Mg–Si alloy. (a) Before immersion and (b) corrosion in chloride solution.

With an increase in the concentration of OH^- and Al^{3+} , the reaction activation between Al^{3+} and OH^- increases sharply, forming flocculent insoluble hydroxide sediment [23].



A corrosion schematic diagram of Al–Mg–Si alloys is presented in figure 6. Therefore, increasing the Cl^- concentration is beneficial to increase the corrosion rate by facilitating the process of the corrosion reaction (including chemical and electrochemical reactions), resulting in intense pitting corrosion. In addition, Cl^- penetrating into the tip of corrosion pit can form a local strong acid environment by combination with H^+ , which would promote the in-depth development of the corrosion tip into the alloy interior along the corrosion pathway.

4. Conclusions

The corrosion behaviour of Al–Mg–Si alloys in neutral NaCl solutions has been systematically studied. It has been found that the corrosion of the alloys in sodium chloride solution is caused by chemical and electrochemical reactions, and no change in the corrosion mechanism occurs due to the variation in NaCl concentration. But the corrosion rate is significantly different. The effects of chloride on the corrosion behaviours and the electrochemical properties of the Al–Mg–Si alloys are summarized as follows.

In 2 wt.% NaCl solution, slight pitting corrosion appears around the MgSi particles on the grain boundaries; when NaCl concentration increases up to 3.5 wt.%, the alloy presents severe pitting corrosion and intergranular corrosion. In 5 wt.% NaCl solution, the alloy presents serious overall corrosion, where the grain and grain boundaries are all corroded.

With an increase in NaCl concentration, the corrosion rate of the Al–Mg–Si alloy sharply increases by enhancing the driving force of chemical and electrochemical dissolutions, E_{corr} and E_{pit} , shift to a more negative value, and i_{corr} increases. In 5 wt.% NaCl solution, the passivation platform of the potentiodynamic polarization becomes inconspicuous.

References

- [1] Verma C, Ebenso E E and Quraishi M A 2017 *J. Mol. Liq.* **233** 403
- [2] Liu H W, Xu D, Dao A Q, Zhang G, Lv Y L and Liu H F 2015 *Corros. Sci.* **101** 84
- [3] Tomashov N D 1958 *Corrosion* **14** 39
- [4] Farhad B, Mohiedin B H, Samin S, Yadollah Y, Golsa Mor-tazavi M and Seo Y 2016 *Met. Mater. Int.* **22** 609
- [5] Ai Z Y, Sun W, Jiang J Y, Song D, Ma H, Zhang J C *et al* 2016 *Materials* **9** 749
- [6] Li S J, Sun W, Yang Z Q, Zhang X Y, Wang L D and Liu G C 2018 *Electrochim. Acta* **292** 425
- [7] Fermamdes J C S, Picciochi R, Cunhabelo M D, Silva T M, Ferreira M G S and Fonseca I T E 2004 *Electrochim. Acta* **49** 701
- [8] Zou Y, Liu Q, Jia Z, Yuan Y, Ding L P and Wang X L 2017 *Appl. Surf. Sci.* **405** 489
- [9] Lim A B Y, Neo W J, Yauw O, Chylak B, Gan C L and Chen Z 2016 *Microelectron. Reliab.* **56** 155
- [10] Zheng Y, Xiao W L, Ge S J, Zhao W T, Hanada S J and Ma C L 2015 *J. Alloys Compd.* **649** 291
- [11] Zheng Y Y, Luo B H, Bai Z H, Wang J and Yin Y 2017 *Metals (Basel)* **7** 387
- [12] Nabhan D, Kapusta B, Billaud P, Colas K, Hamon D and Dacheux N 2015 *J. Nucl. Mater.* **457** 196
- [13] Li Y, Hung Y C, Du Z Y, Xiao Z B and Jia G Z 2018 *Phys. Metals Metallogr.* **119** 339
- [14] Chung I C, Chung C K and Su Y K 2017 *Surf. Coat. Technol.* **313** 299
- [15] Bai Z H, Xia Y M, Qiu F, Liu Y Y, Hu W and Jiang Q C 2014 *Appl. Surf. Sci.* **307** 153
- [16] Tan Y J, Bailey S and Kinsella B 1996 *Corros. Sci.* **38** 1545
- [17] Guan L, Zhou Y, Zhang B, Wang J Q, Han E H and Ke W 2016 *Corros. Sci.* **103** 255
- [18] Huang W, Hurley B L, Yang F and Buchheit R G 2016 *Electrochim. Acta* **199** 242
- [19] Shi Y, Liu L, Zhang, L, Li R and Yu B 2017 *J. Iron Steel Res. Int.* **24** 957
- [20] Liu Y, Zhou X, Thompson G E, Hashimoto T, Scamans G M and Afseth A 2007 *Acta Mater.* **55** 353
- [21] Amina M A, Abd El-Rehima S S and El-Lithy A S 2010 *Electrochim. Acta* **55** 5996
- [22] Thomas S, Medhekar N V, Frankel G S and Birbilis N 2015 *Curr. Opin. Solid St M.* **19** 85
- [23] Amin M A 2010 *Corros. Sci.* **52** 3243